Dynamical Study of H_2 and D_2 Desorbing from a Cu(111) Surface†

Aurelie Perrier,* Laurent Bonnet, and Jean-Claude Rayez

Laboratoire de Physico-Chimie Moleculaire, UMR 5803, Universite Bordeaux 1 and CNRS, 33405 Talence Cedex, France

Received: July 27, 2005; In Final Form: October 28, 2005

A theoretical study of H_2 and D_2 desorbing from Cu(111) is reported. The study makes use of the LEPS PES of Dai and Zhang [*J. Chem. Phys.* **1995**, *102*, 6280]. The LEPS parameters have been modified in order to lower the barrier threshold in conformity with accurate ab initio electronic structure calculations. The topological study of the modified PES by the CHAIN method reveals unambiguously that the transition state (TS) is located at the top of a unique early barrier along the desorption path. The adsorbed H atoms are supposed to be in thermal equilibrium with the metal surface. Batches of classical trajectories (CT) are then carried out from the TS onto the products with their initial conditions canonically distributed and the effect of their possible recrossing of the TS taken into account according to Keck's method [*Discuss. Faraday Soc.* **1962**, *33*, 173]. Product state distributions are then calculated using the Gaussian weighting procedure [*Chem. Phys. Lett.* **2004**, *397*, 106] to account for the quantization of the vibration motion of the desorbed diatom. These distributions are in overall good agreement with experimental measurements. On average, the early barrier to desorption results in a significant vibrational excitation of the final diatom and a strong deexcitation of its rotational angular momentum *J* from the TS onto the products. Moreover, the orientation of the rotation plane is roughly random for low values of *J* (both cartwheel and helicopter motions are observed) while it is more likely parallel to the metal surface for large values of *J* (predominance for helicopter motion). These findings are analyzed in some details.

1. Introduction

Associative desorptions are fundamental processes in gas−surface chemistry. This is why their dynamics has been widely studied both experimentally and theoretically during the last 50 years.[1,2] Many of these works concern the recombinative desorption of H_2 and D_2 from Cu(111) and Cu(110); the H_2/Cu system is in fact considered as an important model system for the understanding of activated gas−surface reactions.

Internal state distributions of H_2 and D_2 associatively desorbing from Cu(111) and Cu(110) have been measured by different groups.[3−10] In these experiments, H and D atoms, after permeating through a Cu crystal, recombine at the metal surface and desorb. The desorbing molecules are detected in a state-specific manner using resonance enhanced multiphoton ionization (REMPI) combined with mass spectroscopy. It is also possible to determine the preferential steric orientation of the desorbing molecules by measuring its rotational quadrupole alignment.[11−13] In other words, one may measure the propensity of the final diatom to rotate in a plane parallel to the metal surface ("helicopter" motion) or perpendicular to it ("cartwheel" motion). The results of these experiments have shown that the distributions of the observables are nonstatistical. For instance, the desorbed molecules present a significant vibrational and translational excitation with respect to Boltzmann expectations. Besides, the mean translational energy is a decreasing function of the vibrational state and a nonmonotonic function of the rotational state *J*[8−10] while it should be independent of them for a purely statistical desorption. It seems also that the higher *J*, the larger the preference for helicopter motion (again a nonstatistical behavior).

From the theoretical side, only reduced-dimensionality calculations have been performed to date, as far as desorptions is concerned. Earliest classical trajectory calculations[14,15] reproduced qualitatively the essential features of the experimental observations related to the translational and vibrational energy distributions of the desorbed H_2 molecules. These calculations focused on the vibrational energy of the desorbed molecules and used a model two-dimensional potential energy surface (PES). Since the rotation motion was kept uncoupled with the translation and vibration motions from the barrier top onto the products, the rotational energy distribution remained Boltzmannian beyond the barrier top, in contradiction with experimental results. More recent classical trajectory calculations[16] used a 3-dimensional model PES where two types of coupling were introduced: a coupling between the translational and vibrational degrees of freedom, and a coupling between the translational and the cartwheel type degrees of freedom. These classical trajectory calculations showed that there is a rotational deexcitation between the transition state (TS) and the products, and also that the desorbed molecules preferentially exhibit a helicopter-like motion. Their study, however, does not take into account the coupling between the helicopter type degree of freedom and the remaining coordinates.

Time independent quantum calculations of the desorption probability were also performed by neglecting the translation motions parallel to the surface (see refs 17 and 18 and references therein). Moreover, these calculations focused on the rotational effects in the associative desorption dynamics of D_2 and H_2 on Cu(111) and no indication concerning the translational and vibrational energy distributions is given.

† Part of the special issue "William Hase Festschrift".

* Corresponding author. E-mail: a.perrier@lpcm.u-bordeaux1.fr.

10.1021/jp054143p CCC: $33.50
Published on Web 11/30/2005

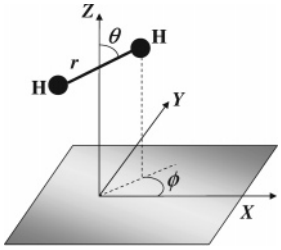

Figure 1. Coordinate system for the H_2 + Cu(111) system.

Therefore, no theoretical study gives a complete description of internal state distributions of H_2 or D_2 desorbing from a Cu(111) surface and existing results are only in partial agreement with experimental features. This is why in this paper, we report a full dimensional dynamical study of the desorption of H_2 and D_2 from a Cu(111) surface with a systematic comparison with existing data.

The paper is organized as follows. In section 2, we present the system under scrutiny as well as the *ab* initio PES used in the dynamical calculations. Section 3 deals with the details of the classical trajectory (CT) calculations. Comparisons between experimental data and CT results as well as their discussion is performed in section 4. We conclude in section 5.

2. The H_2/Cu(111) System

H_2 is defined by the following set of 12 canonical coordinates (X, P_X, Y, P_Y, Z, P_Z, r, p_r, θ, p_θ, ϕ, p_ϕ). X and Y are the coordinates of the center of mass G of the molecule in a plane parallel to the surface, Z is the distance between G and the surface, r is the distance between the two atoms, θ is the angle between the molecule and the surface normal, and ϕ is the azimuthal angle [see Figure 1]. θ and ϕ are associated with the cartwheel and helicopter motions, respectively. P_X, P_Y, P_Z, p_r, p_θ, and p_ϕ are the conjugate momenta of the previous space coordinates. The classical function of Hamilton can be written as

$$H = \frac{P_X^2 + P_Y^2 + P_Z^2}{2M} + \frac{p_r^2}{2\mu} + \frac{J^2}{2I} + V \qquad (2.1)$$

with

$$J^2 = p_\theta^2 + \frac{p_\phi^2}{\sin^2\theta} \qquad (2.2)$$

and

$$I = \mu r^2 \qquad (2.3)$$

M and μ are respectively the mass and the reduced mass of H_2. J is the rotational angular momentum of H_2, and I is its reduced moment of inertia. The potential energy V is zero for Z tending to infinity and r equal to r_e, the equilibrium bond distance of the free H_2 (r_e = 0.742 Å).

Surface degrees of freedom are not taken into account in this study. As we shall see in the following, classical trajectory calculations are only carried out from the barrier top onto the products. During this stage, the very light H_2 or D_2 molecules recoil from the surface with a large velocity as compared with the velocity of the much heavier Cu atoms. For such a reason, we believe that keeping the Cu atoms at their mean positions, coinciding with their equilibrium positions is a good approximation.

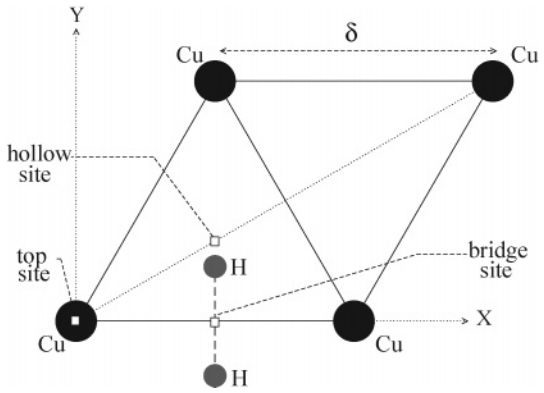

Figure 2. High-symmetry sites (top, bridge, hollow) on the Cu(111) surface. These sites are represented by open squares. δ corresponds to the smallest distance between two Cu atoms (δ = 2.56 Å). The projection of the position of the two H atoms at the TS ($X^\ddagger = \delta/2$, $Y^\ddagger = 0$, $Z^\ddagger$ = 1.26 Å, $r^\ddagger$ = 1.03 Å, $\theta^\ddagger = \pi/2$, and $\phi^\ddagger = \pi/2$) is also depicted.

To describe the interaction V between the H atoms and the Cu(111) surface, we have used a LEPS potential energy surface built by Dai and Zhang.[19] This 6D PES was based on density functional calculations (GGA approximation) performed by Hammer et al.[20] To describe the corrugation of the surface, the atom−surface potential parameters of this PES are dependent on the surface site. The Sato parameters were adjusted to reproduce the barrier height (0.720 eV in the LEPS−PES vs 0.730 eV in the DFT calculations) and the barrier location (Z = 1.2 Å and r = 1.1 Å) for the bridge-to-hollow dissociation geometry for which Hammer et al. found the lowest reaction barrier.

However, the DFT-GGA barrier (0.730 eV) obtained by Hammer et al.[20] is too high. The same authors performed convergence tests showing indeed that increasing the number of electronic states in the calculations lowers the barrier height by about 0.2 eV. Hence, the LEPS−PES[19] whose parameters are fitted to reproduce the DFT-GGA barrier overestimates the minimum threshold to dissociation. Accordingly, we adjusted the LEPS parameters to lower the barrier without modifying its position. We found that a good compromise was to lower the dissociation energies of the Morse functions describing the atom−surface interactions. The three atom−surface dissociation energies used in the LEPS PES (corresponding to three symmetric sites top, bridge and hollow) were shifted down by 0.05 au, i.e., 0.136 eV.

To check that the topology of the PES was unchanged, except the barrier height, the potential calculation was implemented in the AMPAC 7.25 package.[21] The possible reaction paths between the adsorbed phase (two H atoms adsorbed on the surface) and the gas phase were then determined using the CHAIN method.[22,23] Briefly, this method consists of (a) defining a reactant and a product configuration, (b) generating a series of geometries forming a smooth continuous path between the two previous configurations, and (c) relaxing the geometries in directions perpendicular to the chain path. For activated processes, this procedure, detailed in refs. 22 and 23 (see also ref. 24), leads to the saddle point corresponding to the highest energy along the relaxed path (other saddle points may exist along the relaxed path but their energy is lower). This method was previously used to characterize the topology of the H_2/Pt(111) PES.[25,26] Product configurations were defined by $Z^\ddagger$ = 6 Å, $r = r_e$ and a random selection of X, Y, θ, and ϕ. The set of adsorbed configurations was determined as follows: each of the two H atoms was localized in a high-symmetry site (top, bridge, hollow as shown on Figure 2) within the restriction that

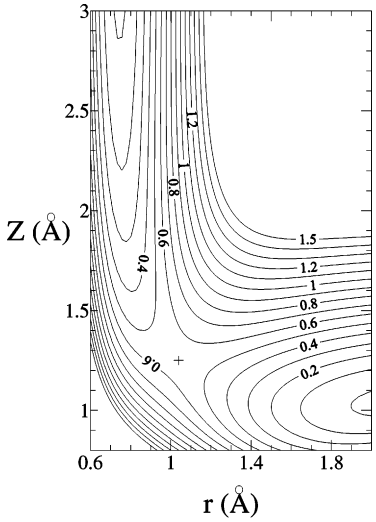

Figure 3. Contour plot representation in the (r, Z) plane of the modified LEPS PES used in the calculations. The center of mass of the molecule is located over a bridge site with $\theta = \pi/2$ and $\phi = \pi/2$. The energy level spacing is 0.1 eV. The cross in the figure represents the saddle point.

the distance r between the two atoms was lower than 5 Å. We used this restriction in order to limit the number of possible adsorbed configurations. Each configuration was then optimized using the "trust radii" method (see ref.[24] and references therein). We then ran a batch of 500 CHAIN calculations, each one joining one adsorbed minimum to a random gas phase configuration. All these calculations led to a single saddle point. This point is precisely defined by $X^{\ddagger} = 1.28$ Å, $Y^{\ddagger} = 0$, $Z^{\ddagger} = 1.26$ Å, $r^{\ddagger} = 1.03$ Å, $\theta^{\ddagger} = \pi/2$ and $\phi^{\ddagger} = \pi/2$. The center of mass of H_2 is thus located over a bridge site (see Fig. 2). The values of $X^{\ddagger}$, $Y^{\ddagger}$, $\theta^{\ddagger}$ and $\phi^{\ddagger}$ were unmodified with respect to the original PES while we observe a small variation of $Z^{\ddagger}$ and $r^{\ddagger}$. $Z^{\ddagger}$ was shifted from 1.21 Å for the original LEPS PES to 1.26 Å for the modified one, and $r^{\ddagger}$ decreases from 1.10 to 1.03 Å. The topology of the PES is thus quasiunchanged, and the coordinates of the one and only saddle point are very close to the coordinates of the original one. The energy difference between this saddle point and the H_2 molecule at equilibrium in the gas phase is $V^{\ddagger} = 0.562$ eV instead of 0.720 eV for the unmodified PES. As can be seen in Figure 3, the desorption barrier defined by this saddle point is located in the entrance channel. The desorption of H_2 from Cu(111) is thus characterized by an early barrier.

The eigenvectors ($\bar{U}_i$ with $i = 1-6$) of the mass-weighted Cartesian Hessian matrix were calculated at the saddle point. In the neighborhood of this point, the reaction coordinate was defined by the eigenvector with the negative eigenvalue ($\bar{U}_1$). We have thus defined the TS as the planar hypersurface of the phase space which is orthogonal to the vector $\bar{U}_1$ and which projection onto the configuration space contains the saddle point (SP). Our description of the TS does not correspond to the rigorous definition, i.e. the minimum of the desorption flux in phase space. However, localizing the TS at the top of the barrier is a good approximation for activated processes (see refs 27 and 28 and references therein).

In the neighborhood of the saddle point, H_2 can be defined by a new set of canonical coordinates (u_i, p_i), with $i = (1, ..., 6)$, where u_i is the space coordinate of H_2 along the vector $\bar{U}_i$ and p_i is its conjugate momentum. The saddle point SP is defined by $u_i = 0$ for $i = (1, ..., 6)$. Using this coordinate system, the Hamiltonian [eq 2.1] becomes

$$H = \sum_{i=1}^{6} \frac{p_i^2}{2} + V \tag{2.4}$$

Our planar approximation P of the TS is therefore $u_1 = u_1^{\ddagger} = 0$.

3. Methodology

3.1. Desorption Flux According to Keck's Method. While adsorbed on the Cu(111) surface, the two hydrogen atoms are in thermal equilibrium, at temperature T_s, with the metal surface. In the framework of the coordinate system previously introduced, the classical equilibrium desorption flux is rigorously given by[29−32]

$$F^{\ddagger}(T_s) \propto \int \mathrm{d}\mathbf{u}\, \mathrm{d}\mathbf{p}\, \mathrm{d}p_1\, p_1 \exp[-\beta H(u_1 = 0, \mathrm{u}, p_1, \mathbf{p})]\, \Theta(p_1) \xi(\mathbf{u}, p_1, \mathbf{p}) \tag{3.1}$$

with $\mathbf{u} = (u_2, u_3, u_4, u_5, u_6)$, $p = (p_2, p_3, p_4, p_5, p_6)$, H defined in eq 2.4, Θ the Heaviside function, and β equal to $1/(k_B T_s)$ with k_B the Boltzmann constant. $\xi(\mathbf{u}, p_1, \mathbf{p})$ is zero if the trajectory crossing P with $\mathbf{u}$, a positive value of p_1 and $\mathbf{p}$ goes back to the reagents (reagents were considered to be formed when r is larger than 2 Å) or comes initially from the products through direct scattering. It is the inverse of the number of crossing in the product direction for the remaining trajectories, which come from the reagents and end in the products (products were considered to be formed when Z is larger than 5 Å) In order to calculate $\xi(\mathbf{u}, p_1, \mathbf{p})$, trajectories are thus run from the hypersurface P in both the future and the past until either the products or the reagents are reached. This method was introduced by Keck in the early 1960s[29] and subsequently used and developed by several authors.[30,33] It turns out, however, that recrossings are negligible (see further below).

The initial conditions of the n th reactive trajectory, namely, $u_1 = 0$, p_1^n ($p_1^n \geq 0$), $\mathbf{u}^n$ and $\mathbf{p}^n$, are randomly assigned and its statistical weight is therefore

$$W^{\ddagger n} = p_1^n \exp[-\beta H(u_1 = 0, \mathrm{u}^n, p_1^n, \mathbf{p}^n)] \xi(\mathrm{u}^n, p_1^n, \mathbf{p}^n) \tag{3.2}$$

We know the phase space coordinates of the H_2 system in the Hessian eigenvector basis set. For convenience, we shall integrate the equations of motion in Cartesian coordinates, for this is the physical space. The initial phase space coordinates of H_2 are thus transformed from the Hessian eigenvector basis set to the Cartesian coordinate basis set. Moreover, to calculate the partition of the total energy among the different degrees of freedom, the values of the internal coordinates (X, Y, Z, r, θ, ϕ) and their corresponding momenta are determined. Some details about these transformations are given in the appendix.

The total energy of each trajectory was allowed to vary between the value of the potential barrier $V^{\ddagger}$ and $V^{\ddagger} + 10kT_s$, a value above which the weighting factor is negligible.

It should be noted that among the trajectories contributing to the flux (eq 3.1), a few ones might correspond to an Eley−Rideal (ER) process while the experiment we wish to simulate can only produce Langmuir−Hinshelwood (LH) type of trajectories.[4,10] As stated previously, however, we do not run trajectories in the past for a long time so that we do not know if the trajectories considered correspond to ER or LH processes.

Nevertheless, the percentage of ER events should be tremendously lower than the one of LH events for the following reason: the system under scrutiny is roughly comparable to a microcanonical (conservative) system made of two H atoms interacting with an enormous metal cluster in the vacuum. There are four asymptotic channels corresponding, respectively, to the H_2 molecule far from the cluster (channel 1), two H atoms far from each other and the cluster (channel 2), and one H atom adsorbed on the cluster while the second is far from it (channels 3 and 4). For such a system, the LH mechanism can be viewed as the second step of a long-lived collision coming from any channel and ending in channel 1 while the ER mechanism corresponds to a fast passage from channel 3 or 4 to channel 1. Now, consider the reverse processes, i.e., reactions from channel 1 to any channel. Given the number of degrees of freedom of the system and the strong couplings between them when the two H atoms are adsorbed on the cluster, the classical dynamics in the strong coupling region (SCR) are chaotic. The system wanders about the phase space corresponding to this region and the probability of dissociation decreases exponentially in time from a given instant t_0 to infinity. $t = 0$ corresponds to the crossing of the TS separating channel 1 from the SCR and t_0 corresponds to the instant where the first dissociations of the intermediate complex occur, part of them leading to channels 3 or 4. t_0 is expected to be equal to a few tenths of femtoseconds, which corresponds to a reverse ER mechanism involving one rebound only on the unavailable parts of the phase space region associated with the SCR. Moreover, the average lifetime of the intermediate complex is expected to be orders of magnitude larger than t_0, i.e., the dissociation probability decreases extremely slowly with respect to t_0. One thus expects that trajectories of the reverse ER type will be negligible with respect to those corresponding to an intricate diffusion motion of the H atoms on the cluster surface before the final dissociation. From the microreversibility principle, trajectories of the ER type should thus represent a negligible part of the whole trajectories connecting channels 3 and 4 with channel 1, and a fortiori, a negligible amount of the whole set of trajectories leading to channel 1.

3.2. Product State Distributions. The Hamiltonian function (eq 2.1) can be written as

$$H = H_R + H_V + H_T \tag{3.3}$$

H_R, H_V, and H_T are the rotational, vibrational, and translational Hamiltonians in the separated products respectively defined by

$$H_R = \frac{J^2}{2I} \tag{3.4}$$

$$H_V = \frac{p_r^2}{2\mu} + V \tag{3.5}$$

and

$$H_T = \frac{P_X^2 + P_Y^2 + P_Z^2}{2M} \tag{3.6}$$

I is given by eq 2.3 with r kept at r_e (rigid rotor approximation).

To account for the quantization of the final vibration motion of H_2 (D_2), we shall not work in the framework of the fully classical picture. A convenient way to deal with this quantization is to apply the Gaussian-weighting procedure.[34,35] The product vibration action x is defined by

$$x = \frac{H_V}{\hbar\omega} - \frac{1}{2} \tag{3.7}$$

with ω the vibrational frequency of H_2. For the n th trajectory, another weighting factor is then introduced, namely:

$$\delta_n = \sum_v \delta_v^n \tag{3.8}$$

where v is the vibrational quantum number ($v = 0, 1, ...$) and

$$\delta_v^n = \exp\left[-\frac{(v - x_n)^2}{\epsilon^2}\right] \tag{3.9}$$

is a Gaussian function (x_n is the final vibrational action for the nth trajectory). When the vibrational action is close to an integer value, the weighting factor is large. On the opposite, a vibrational action far from an integer value leads to a weighting factor close to zero. The ϵ parameter of the Gaussian functions was chosen small enough to quantize the vibration motion but sufficiently large to get a satisfying statistics. ϵ was kept at 0.1.

As a consequence of the Gaussian-weighting procedure, the overall weighting factor W^n of the nth reactive trajectory will be given by

$$W^n = \delta_n W^{\ddagger n} \tag{3.10}$$

instead of eq 3.2, which would correspond to a full classical treatment of the whole degrees of freedom.

Gaussian weighting in CT calculations has been recently introduced in gas-phase dynamics and good agreement was found with quantum scattering calculations as far as product state distributions are concerned.[36−41] This method has also been recently applied to the desorption reaction of H_2 from a Pt(111) surface.[26]

To determine the final rotational state distribution, we use a histogram binning procedure since the energy difference between two rotational levels is much smaller than the energy difference between two vibrational states.

4. Comparison between CT Calculations and Experimental Data

Product state distributions of H_2 and D_2 desorbing from Cu(111) were measured for two different surface temperatures T_s, 850 and 925 K. For such relatively high temperatures, we expect that tunneling is very weak and our classical treatment of the dynamics should be satisfying. We shall now compare our CT calculations with the experimental data. Each batch of calculations involved 400 000 trajectories. In each case, around 250 000 trajectories were found to be reactive and 97% of these reactive trajectories connect the reacting zone to the product region without recrossing the planar dividing surface P.

4.1. Vibrational State Population. The vibrational population ratios are given in Table 1. CT calculations are compared with experimental results and with Boltzmann expectations.

We first notice that CT ratios are in satisfying agreement with experimental values. At $T_s = 850$ K, our results are close to the lower limit of the experimental error bar for both H_2 and D_2. At $T_s = 925$ K, our results overestimate the population of the $v = 1$ state for H_2. However, the $P(v=1)/P(v=0)$ ratio measured for a surface temperature of 925 K[4] is surprisingly much smaller than the value of the same ratio measured at $T_s = 850$ K[8] (one would have expected the reverse). Further

TABLE 1: Vibrational Population Ratios of H_2 and D_2 Desorbing from Cu(111) at Two Different Temperatures (T_s = 850 K and T_s = 925 K)[a]

	T_s = 850 K				T_s = 925 K		
	CT	expt	Boltzmann		CT	expt	Boltzmann
				H_2/Cu(111)			
$P(v=1)/P(v=0)$	0.058	0.084 ± 0.030[4]	0.0009		0.073	0.029 ± 0.007[8]	0.0016
				D_2/Cu(111)			
$P(v=1)/P(v=0)$	0.147	0.35 ± 0.20[4]	0.0063		0.162	0.20 ± 0.03[8]	0.010
$P(v=2)/P(v=0)$	0.0008		5×10^{-5}		0.011	0.0096 ± 0.0020[8]	0.0012

[a] Classical trajectory calculations (CT) are compared with experimental data and Boltzmann predictions.

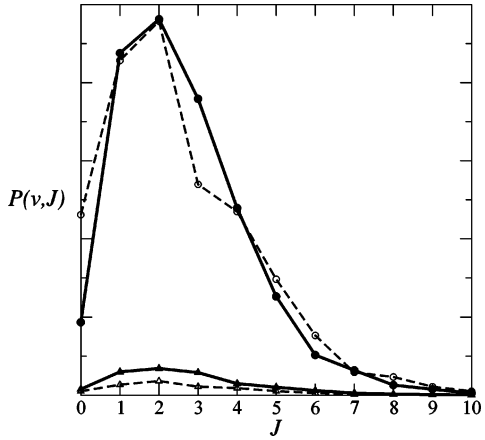

Figure 4. Rovibrational state distribution of H_2 desorbed from Cu(111) at 925 K. CT results are plotted as a function of the rotational state J for different vibrational states (filled circles ($v = 0$) and filled triangles ($v = 1$) connected by solid lines). The experimental results obtained by Rettner et al.[10] are represented by open symbols with dashed lines. These distributions were originally displayed in a plot of $\ln[F_{(v,J)}/(g_n(2J+1))]$ as a function of the rotational energy where $F_{(v,J)}$ is the flux measured for each state, g_n is the nuclear spin degeneracy and $(2J+1)$ is the corresponding quantum rotational degeneracy (see Figure 7 in ref 10). The experimental rovibrational state distribution thus corresponds to the exponential value of the signal $ln[F_{(v,J)}/(g_n(2J+1))]$ multiplied by the corresponding $(2J+1)$ factor.

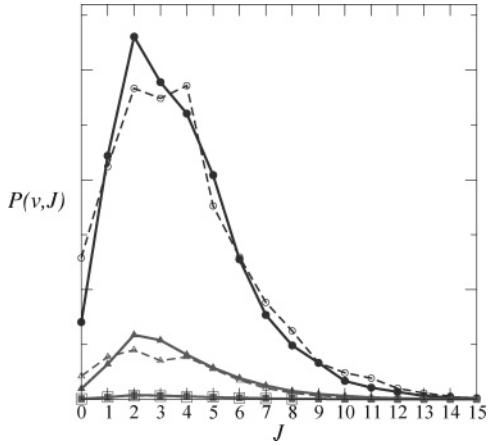

Figure 5. Rovibrational state distribution of D_2 desorbed from Cu(111) at 925 K. CT results are plotted as a function of the rotational state J for different vibrational states (filled circles ($v = 0$), filled triangles ($v = 1$) and filled squares ($v = 2$) connected by solid lines). The experimental results obtained by Michelsen et al.[8] for several vibrational state are represented by open symbols with dashed lines (see Figure 4 for explanations).

experimental studies seem necessary to settle. For D_2, the ratios are in good agreement with experimental data.

Besides, both theory and experiments show a strong vibrational excitation of the desorbing molecule as compared with Boltzmann predictions. As a matter of fact, for D_2 desorbed from Cu(111) at T_s = 925 K, the calculated $P(v=1)/P(v=0)$ and $P(v=2)/P(v=0)$ ratios are consistent with vibrational temperatures of 2360 and 1860 K respectively.

The vibrational excitation of the desorbed molecule can be explained by the early nature of the barrier to desorption (see Figure 3). At the TS, the diatom bond distance ($r^{\ddagger} = 1.03$ Å) is significantly larger than the final equilibrium distance ($r_e = 0.74$ Å). A significant amount of energy is thus stored in the bond coordinate across the barrier descent and part of it is retained into the gas phase. This vibrational excitation is well understood in terms of Polanyi's rules[42] (see also refs 9, 14, 15, 17, 43, 44).

4.2. Rotational State Distributions. The vibrationally resolved rotational state distributions found from CT calculations are compared with the measured ones in Figures 4 and 5. The agreement between both sets of results is very satisfying. This agreement is also displayed in Figure 6 where for the sake of convenience, state distributions are separately represented for each vibrational state.

Figure 7 enables us to straightforwardly compare the CT vibrationally resolved rotational state distributions as well as the rotational state distribution at the TS (all these distributions are normalized to the same area). As a matter of fact, the $v = 0$, $v = 1$, and $v = 2$ final distributions are identical to. Moreover, one can notice that the rotational state distribution is strongly shifted toward the small J values on the way from the TS onto the products. Figure 8 confirms this finding, and provides supplementary information on the shift. This figure shows that the average rotational state $\langle J^{\ddagger} \rangle$ at the TS is systematically larger than the final rotational state J. As shown elsewhere,[45] such a shift of the rotational state distribution is mainly due to energy transfers between rotation and translation motions. These transfers have been discussed at length in gas-phase triatomic and tetraatomic unimolecular reactions[46−49] and the interested reader will find many details in the corresponding references. To last, Figure 8 shows that, as the final value of J increases ($J > 8$), the average value of $J^{\ddagger}$ gets closer to the value of J in the gas phase. The reason is that the molecules which are rotationally excited at the TS are less sensitive to the anisotropy of the PES than those which are not. Their rotational state is thus less modified from the TS on.

4.3. Translational Energy Distribution. The average value of the translational energy is depicted in Figures 9 and 10 for H_2 and D_2 desorbing from Cu(111) at T_s = 925 K. The mean translational energy is plotted as a function of the rotational angular momentum J for the different vibrational states available.

As can be observed, there is a semiquantitative agreement between theory and experiment.[9] If we average over all quantum states, we find for instance that for D_2, the mean translational energy is 0.65 eV while the value measured by Michelsen et al.[7] is 0.58 ± 0.05 eV. The overestimate of the barrier height, 0.562 eV for the modified LEPS PES while the advanced DFT

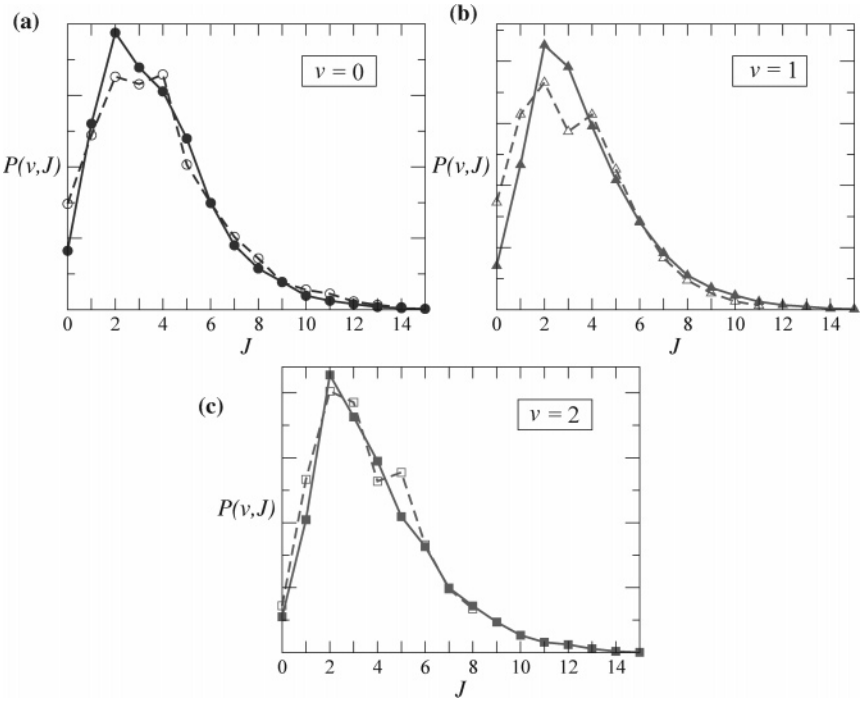

Figure 6. Like Figure 5, except that the three vibrational state resolved distributions are separated and equally normalized.

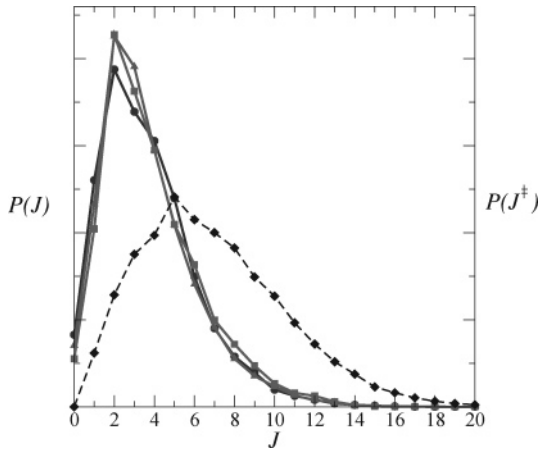

Figure 7. Rotational state distribution of D_2 desorbed from Cu(111) at 925 K. Results are plotted as a function of the rotational state J for different vibrational states (filled circles ($v = 0$), filled triangles ($v = 1$), and filled squares ($v = 2$) connected by solid lines). The distribution at the TS is also depicted (dashed curve with diamonds).

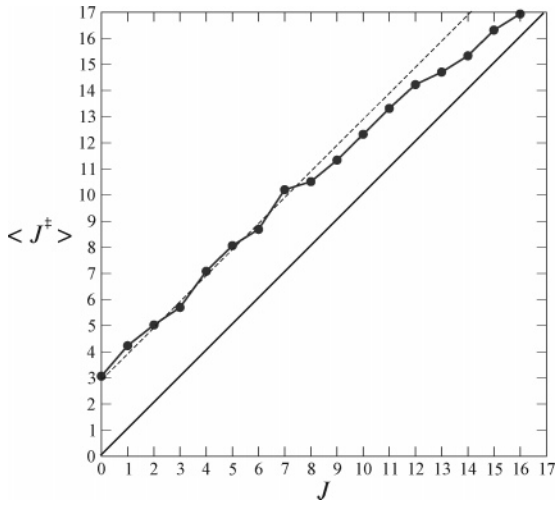

Figure 8. Average value of the rotational state $J^{\ddagger}$ at the TS ($D_2(v{=}0)$ desorbed from Cu(111) at $T_s = 925$ K) plotted as a function of the rotational state in the products. The solid line ($\langle J^{\ddagger}\rangle = J$) and the dashed line are guides for the eyes.

calculations[20] suggest a dissociation threshold close to 0.500 eV, may explain the overvaluation of the CT translational energy. The variation of the mean translational energy as a function of the vibrational and rotational state is well reproduced. For both H_2 and D_2, the mean kinetic energy of the molecule decreases as the vibrational state v increases and is a nonmonotonic function of the rotational state.

The dependence of the mean value of the translational energy on both the vibrational state and the rotational state will be discussed in a future work.

4.4. Rotational Alignment. The average rotational quadrupole alignment $A_0^{(2)}(J)$ reveals information on the alignment of molecules desorbing from a surface with a rotational angular momentum J. This quantity is defined by[50]

$$A_0^{(2)}(J) = \langle 3\cos^2\Xi - 1\rangle_J \tag{4.1}$$

where Ξ is the angle between the rotational angular momentum vector and the Z axis. By introducing the definition of the angle Ξ, $A_0^{(2)}(J)$ can be written as[50]

$$A_0^{(2)}(J) = \left\langle \frac{3m^2 - J(J+1)}{J(J+1)} \right\rangle_J \tag{4.2}$$

where m is the quantized projection on the Z axis of the rotational angular momentum in $\hbar$ units.

In classical mechanics, this quantity becomes

$$A_0^{(2)}(J) = \left\langle \frac{3J_z^2 - J^2}{J^2} \right\rangle_J \tag{4.3}$$

where J_z is the projection of the rotational angular momentum vector on the Z axis.

A positive/negative value of $A_0^{(2)}(J)$ corresponds to a preferential alignment of the rotational angular momentum

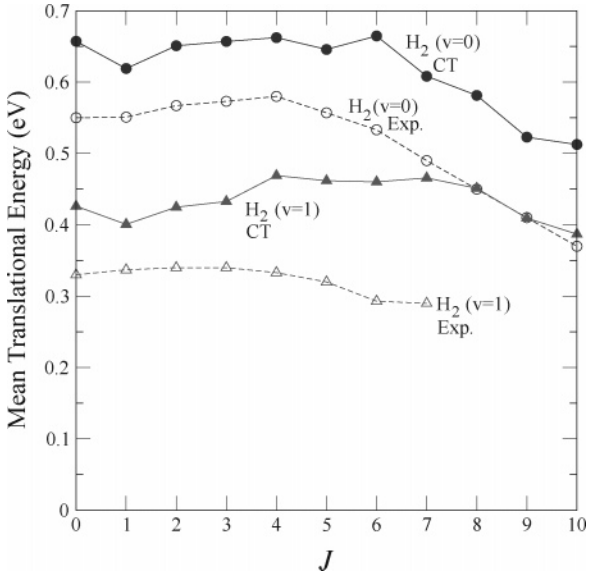

Figure 9. Mean translational energy of H_2 desorbed from Cu(111) at 925 K. Results are plotted as a function of the rotational state J for different vibrational states. Results obtained by CT calculations are represented by filled symbols with solid lines. Experimental results obtained by Rettner et al.[9] are represented by open symbols with dashed lines.

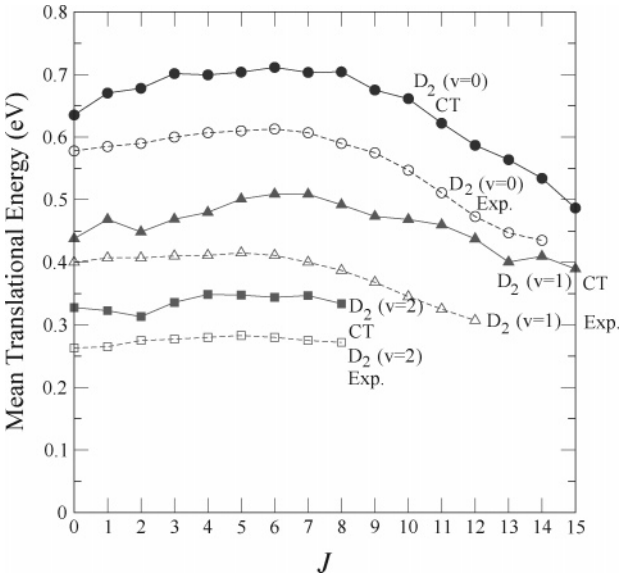

Figure 10. As in Figure 9 for D_2 desorbed from Cu(111) at 925 K.

perpendicular/parallel to the surface. This corresponds to helicopter/cartwheel motion, on average. Since classically, J_z varies from 0 to J, $A_0^{(2)}(J)$ ranges from -1 for a purely cartwheel motion to $+2$ for a purely helicopter motion.

For $D_2(v{=}0,1)$ desorbed from Cu(111) at $T_s = 925$ K, the values of $A_0^{(2)}(J)$ found from CT calculations are depicted in Figure 11 and compared with the experimental results of Gulding et al.[12] Gulding et al. measured the average alignment, by using the REMPI detection technique, for both the P and R branches of $D_2(v{=}0,v{=}1)$ desorbed from Cu(111) at $T_s = 920$ K. The agreement is qualitatively correct. The theoretical alignment is however a bit more excited than the experimental ones. We also notice that our CT calculations are in good agreement with the four-dimensional quantum dynamics results performed by Dino et al. (see Figure 33 in ref 18).

We wish now to understand why the average alignment increase in terms of J. The answer to this question is somewhat

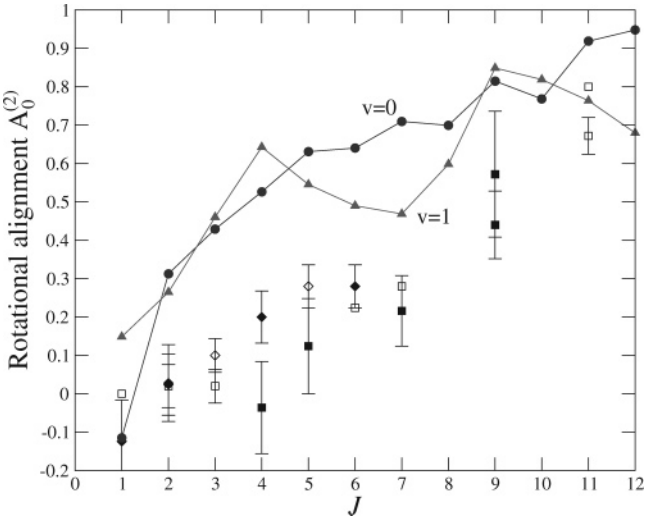

Figure 11. Vibrationally resolved average value of the rotational alignment $A_0^{(2)}(J)$ of D_2 desorbed from Cu(111) at $T_s \simeq 925$ K as a function of the rotational state. CT predictions: filled circles ($v = 0$) and filled triangles ($v = 1$) connected by solid lines. Experimental results (REMPI detection[12]): filled and open squares, $v = 0$, P and R branch transitions respectively; filled and open diamonds, $v = 1$, P and R branch transitions, respectively.

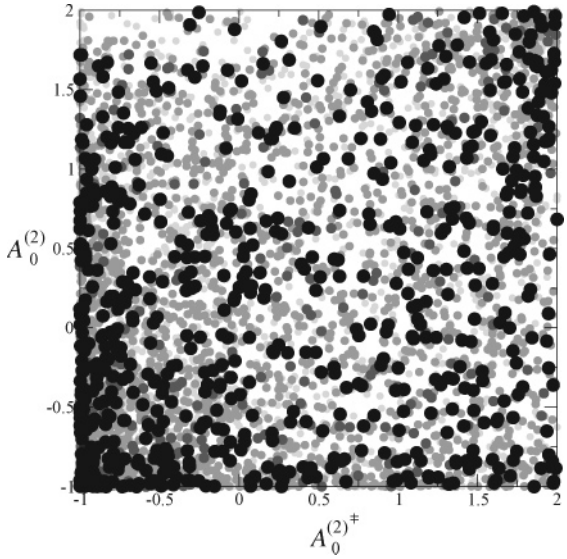

Figure 12. Rotational alignment $A_0^{(2)}$ in the products plotted as a function of the rotational alignment $A_0^{(2)\ddagger}$ at the transition state for trajectories reaching the products with $J = 2$. D_2 desorbed from Cu(111) at $T_s = 925$ K. The darkness of the dots is proportional to the weighting factor of the corresponding trajectory.

subtle and requires first the examination of Figures 12 and 13 in which the final alignment

$$A_0^{(2)} = A_0^{(2)}(J, J_z) = \frac{3J_z^2 - J^2}{J^2} \qquad (4.4)$$

is represented in terms of the alignment at the TS

$$A_0^{(2)\ddagger} = A_0^{(2)\ddagger}(J^\ddagger, J_z^\ddagger) = \frac{3J_z^{\ddagger 2} - J^{\ddagger 2}}{J^{\ddagger 2}} \qquad (4.5)$$

for trajectories reaching the products with $J = 2$ (case I) and $J = 12$ (case II). $J_z^\ddagger$ in eq 4.5 is the projection of the rotational angular momentum vector at the TS on the Z axis.

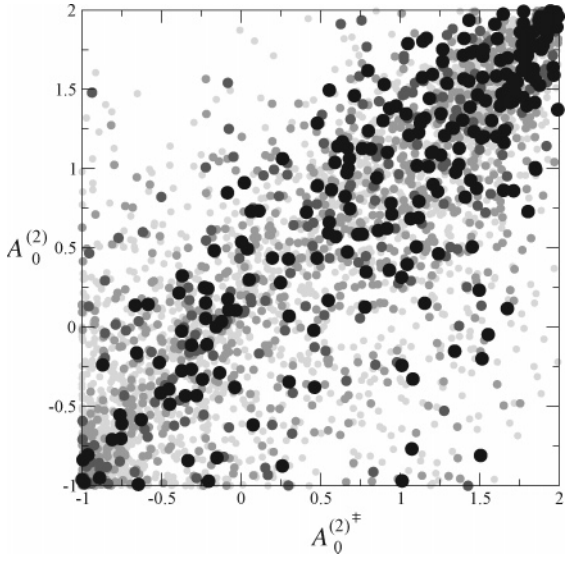

Figure 13. Rotational alignment $A_0^{(2)}$ in the products plotted as a function of the rotational alignment $A_0^{(2)\ddagger}$ at the transition state for trajectories reaching the products with $J = 12$. D_2 desorbed from Cu(111) at $T_s = 925$ K. The darkness of the dots is proportional to the weighting factor of the corresponding trajectory.

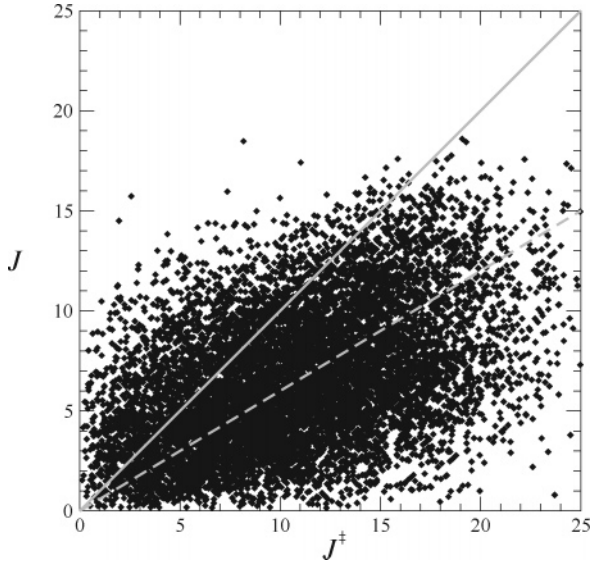

Figure 14. Angular momentum J in the products plotted as a function of the angular momentum $J^\ddagger$ at the transition state for trajectories reaching the products with $-1.0 \leq A_0^{(2)}(J) \leq -0.8$ ("cartwheel" trajectories). D_2 desorbed from Cu(111) at $T_s = 925$ K. Solid line: $J = J^\ddagger$; dashed line: $J = 0.6\ J^\ddagger$.

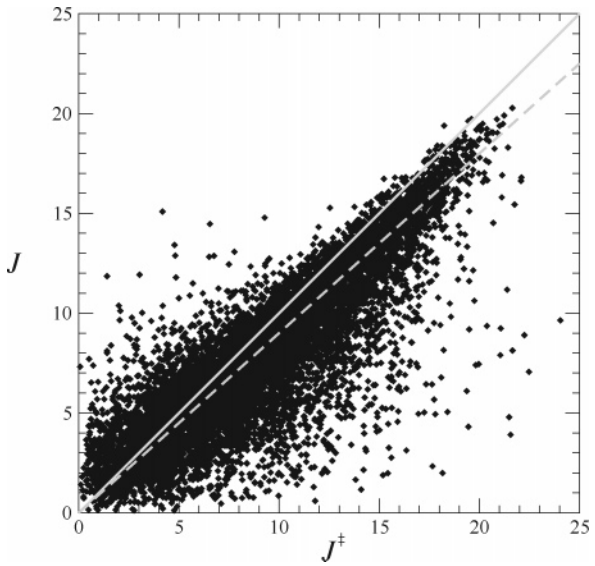

Figure 15. Angular momentum J in the products plotted as a function of the angular momentum $J^\ddagger$ at the transition state for trajectories reaching the products with $1.8 \leq A_0^{(2)}(J) \leq 2.0$ ("helicopter" trajectories). D_2 desorbed from Cu(111) at $T_s = 925$ K. Solid line: $J = J^\ddagger$. Dashed line: $J = 0.9\ J^\ddagger$.

In case I, Figure 8 shows that the average value of $J^\ddagger$ is ~5. Since this value is rather small, the molecule rotates slowly while leaving the TS. In the first instants, it is thus highly sensitive to the anisotropy of the PES. A very weak correlation is expected between $A_0^{(2)}$ and $A_0^{(2)\ddagger}$, as shown by the quasi uniform points distribution displayed in Figure 12. Due to a slightly larger statistical weight in the region corresponding to trajectories exhibiting a cartwheel motion both at the TS and in the products, the average alignment is close to zero (see Figure 11).

In case II, Figure 8 shows that the average value of $J^\ddagger$ is ~14. Since this value is rather high, the molecule rotates quickly while leaving the TS. In the first instants, it is thus less sensitive to the anisotropy of the PES than in case I. A strong correlation is expected between $A_0^{(2)}$ and $A_0^{(2)\ddagger}$, as shown in Figure 13 by the high density of points along the bisector axis. We note, however, that the statistical weight in the region corresponding to trajectories exhibiting a helicopter motion is larger than the one corresponding to trajectories exhibiting a cartwheel motion. The average alignment is therefore larger than in case I, close to 1.

To understand this, consider Figure 14 and Figure 15 in which the final value J of the rotational angular momentum is given as a function of its value $J^\ddagger$ at the TS for trajectories respectively reaching the products with cartwheel and helicopter motions. Figure 14 shows that for cartwheel trajectories, the rotation motion is strongly modified beyond the TS since on average, $J = 0.6J^\ddagger$. For the case of interest, i.e., $J = 12$, the average value of $J^\ddagger$ is found by visual inspection to be equal to ~15. The rotation motion at the TS is indeed in a plane orthogonal to the surface, so that it is strongly hindered. As shown in ref 47, the coupling between Z and θ from the TS on leads to strong energy transfers from rotation to translation motion so that the rotational state distribution is shifted toward the small values of J. In the present case, J decreases from ~15 (on average) to 12. On the opposite, Figure 15 shows that for helicopter trajectories, the rotation motion is weakly modified beyond the TS. $J^\ddagger$ has roughly the same value as in the products, i.e., ~ 12. Now, because of the Boltzmann weighting factor, the probability that $J^\ddagger$ is equal to 15 is much lower than the one to be equal to 12. Accordingly, helicopter trajectories are more probable than cartwheel one, thereby justifying the higher probability density in the high alignment region in Figure 12.

To end, we notice in Figure 11 that when J increases, there is a continuous transition between case I and case II, with a monotonic variation of the average alignment.

Conclusion

A theoretical study of H_2 and D_2 desorbing from Cu(111) has been reported. This study makes use of a modified version of the LEPS PES of Dai and Zhang.[19] The LEPS parameters have been modified in order to lower the barrier threshold in conformity with accurate ab initio electronic calculations. The topological study of the modified PES by the CHAIN method reveals unambiguously that the state (TS) is located at the top

of a unique early barrier. The adsorbed H atoms are supposed to be in thermal equilibrium with the metal surface. Moreover, classical trajectories show that recrossing of the TS is negligible. Accordingly, the nascent molecule is supposed to be still thermalized at the TS and batches of classical trajectories (CT) are carried out from the TS onto the products with their initial conditions canonically distributed. Keck's correction for multiple crossings of the TS is used.[29] Product state distributions of the reactive trajectories are then calculated using the Gaussian weighting procedure to account for the quantization of the vibration motion in gas phase.[34,35] These distributions are in overall good agreement with experimental measurements:

(1) The early barrier to desorption results in a significant vibrational excitation of the desorbed molecule.

(2) The rotational state distribution is strongly modified from the TS onto the products. There is actually a deexcitation of the rotational angular momentum in the exit channel due to energy transfers between rotation and translation motions (see also ref 45).

(3) The variation of the mean translational energy is a decreasing function of the vibrational state and a nonmonotonic function of the rotational state.

(4) The orientation of the rotation plane is roughly random for low J values (both cartwheel and helicopter motions are observed) while it is more likely parallel to the metal surface for large J values (predominance of helicopter motions). This finding has been analyzed in terms of the anisotropy of the PES in the exit channel.

Acknowledgment. The authors are grateful to Professor A. Salin, Dr. C. Crespos, and Dr. P. Larrégaray for useful discussions.

Appendix

By calculating the eigenvectors $\bar{U}_i$ of the mass-weighted Cartesian Hessian matrix, one knows the components of these vectors on the weighted Cartesian coordinates basis set. If we call **U** the Hessian eigenvector basis set and **C** the mass-weighted Cartesian coordinate basis set, we have

$$\mathbf{U} = \mathbf{M}\cdot\mathbf{C} \tag{A.1}$$

where **M** is the transformation matrix.

By assigning the values of u_i ($i = 1-6$) to the projections of H_2 (or D_2) coordinates on the vector $\bar{U}_i$ and by using the inverse transformation matrix, one can then easily determine the mass-weighted Cartesian coordinates c_i of the molecule: $c_1 = \sqrt{m_A}\, x_A$, $c_2 = \sqrt{m_A}\, y_A$, $c_3 = \sqrt{m_A}\, z_A$, $c_4 = \sqrt{m_B}\, x_B$, $c_5 = \sqrt{m_B}\, y_B$, and $c_6 = \sqrt{m_B}\, z_B$. A and B denote the two atoms, and m_A and m_B their respective masses.

The calculation of the Cartesian coordinates of the two atoms is then straightforward and by using simple coordinate transformations, one can evaluate the values of the internal coordinates (X, Y, Z, r, θ, ϕ).

If we derive the set of mass-weighted Cartesian coordinates with respect to time, we obtain for each coordinate c_i:

$$\dot{c}_i = \frac{dc_i}{dt} = \sum_{j=1}^{6} \frac{\partial c_i}{\partial u_j}\frac{du_j}{dt} \tag{A.2}$$

The partial derivatives $\partial c_i/\partial u_j$ are obtained from eq A.1.

In the mass-weighted Cartesian coordinates basis set, the Hamiltonian is given by

$$H = \sum_{i=1}^{6} \frac{p_{c_i}^{\,2}}{2} + V \tag{A.3}$$

where p_{c_i} is the conjugated momentum of the coordinate c_i. Therefore, in eq A.2, we have

$$\dot{c}_i = \frac{\partial H}{\partial p_{c_i}} = p_{c_i} \tag{A.4}$$

Moreover, from eq 2.4, we obtain

$$\frac{du_j}{dt} = \dot{u}_j = \frac{\partial H}{\partial p_j} = p_j \tag{A.5}$$

where p_j is defined in section 2. Using eqs A.4 and A.5, eq A.2 thus becomes

$$p_{c_i} = \sum_{j=1}^{6} \frac{\partial c_i}{\partial u_j} p_j \tag{A.6}$$

Therefore, by knowing the values of the momenta p, one can easily determine the values of the different momenta p_c in the mass-weighted Cartesian coordinate basis set. They are straightforwardly deduced in the Cartesian coordinates basis set by: $p_{x_A} = \sqrt{m_A}\, p_{c_1}$, $p_{y_A} = \sqrt{m_A}\, p_{c_2}$, $p_{z_A} = \sqrt{m_A}\, p_{c_3}$, $p_{x_B} = \sqrt{m_B}\, p_{c_4}$, $p_{y_B} = \sqrt{m_B}\, p_{c_5}$ and $p_{z_B} = \sqrt{m_B}\, p_{c_6}$. Using standard transformations, one can then calculate the values of P_X, P_Y, P_Z, p_r, p_θ, and p_ϕ.

References and Notes

(1) Comsa, G.; David, R. *Surf. Sci. Rep.* **1985**, *5*, 145.
(2) Michelsen, H. A.; Rettner, C. T.; Auerbach, D. J. *Springer Series in Surface Sciences*; Springler-Verlag: Berlin, 1994; Vol. 34, p 185.
(3) Comsa, G.; David, R. *Surf. Sci.* **1982**, *117*, 77.
(4) Kubiak, G. D.; Sitz, G. O.; Zare, R. N. *J. Chem. Phys.* **1985**, *83*, 2538.
(5) Michelsen, H. A.; Auerbach, D. J. *J. Chem. Phys.* **1991**, *94*, 7502.
(6) Rettner, C. T.; Michelsen, H. A.; Auerbach, D. J. *Phys. Rev. Lett.* **1992**, *68*, 1164.
(7) Michelsen, H. A.; Rettner, C. T.; Auerbach, D. J. *Phys. Rev. Lett.* **1992**, *69*, 2678.
(8) Michelsen, H. A.; Rettner, C. T.; Auerbach, D. J.; Zare, R. N. *J. Chem. Phys.* **1993**, *98*, 8294.
(9) Rettner, C. T.; Michelsen, H. A.; Auerbach, D. J. *J. Vac. Sci. Technol. A* **1993**, *11*, 1901.
(10) Rettner, C. T.; Michelsen, H. A.; Auerbach, D. J. *J. Chem. Phys.* **1995**, *102*, 4625.
(11) Wetzig, D.; Rutkowski, M.; David, R.; Zacharias, H. *Europhys. Lett.* **1996**, *36*, 31.
(12) Gulding, S. J.; Wodtke, A. M.; Hou, H.; Rettner, C. T.; Michelsen, H. A.; Auerbach, D. J. *J. Chem. Phys.* **1996**, *105*, 9702.
(13) Hou, H.; Gulding, S. J.; Rettner, C. T.; Wodtke, A. M.; Auerbach, D. J. *Science* **1997**, *277*, 80.
(14) Harris, J.; Holloway, S.; Rahman, T. S.; Yang, K. *J. Chem. Phys.* **1988**, *89*, 4427.
(15) Harris, J.; Rahman, T. S.; Yang, K. *Surf. Sci.* **1988**, *198*, 312.
(16) Yang, K.; Rahman, T. S. *J. Chem. Phys.* **1990**, *93*, 6834.
(17) Kasai, H.; Okiji, A. *Prog. Surf. Sci.* **1993**, *44*, 101.
(18) Dino, W. A.; Kasai, H.; Okiji, A. *Prog. Surf. Sci.* **2000**, *63*, 63.
(19) Dai, J.; Zhang, J. Z. H. *J. Chem. Phys.* **1995**, *102*, 6280.
(20) Hammer, B.; Scheffler, M.; Jacobsen, K. W.; Norskov, J. K. *Phys. Rev. Lett.* **1994**, *73*, 1400.
(21) Semichem, Inc., PO Box 1649, Shawnee, KS 66222, 1992−2003.
(22) Liotard, D. A.; Penot, J. P. *Numerical methods in the study of critical phenomena*; Springler-Verlag: Berlin, 1981; page 213.
(23) Liotard, D. A. *Int. J. Quantum Chem.* **1992**, *44*, 723.
(24) Semichem, Inc., PO Box 1649, Shawnee, KS 66222, 1992−2004.
(25) Olsen, R. A.; Busnengo, H. F.; Salin, A.; Somers, M. F.; Kroes, G. J.; Baerends, E. J. *J. Chem. Phys.* **2002**, *116*, 3841.

(26) Perrier, A.; Bonnet, L.; Rayez, J. C. *Surf. Sci.* **2005**, *581*, 189.
(27) Melissas, V. S.; Truhlar, D. G. *J. Phys. Chem.* **1993**, *99*, 1013.
(28) Truhlar, D. G.; Garrett, B. C.; Klippenstein, S. J. *J. Phys. Chem.* **1996**, *100*, 12771.
(29) Keck, J. C. *Discuss. Faraday Soc.* **1962**, *33*, 173.
(30) Bennett, C. H. American Chemical Society: Washington, DC, 1977.
(31) Grimmelmann, E. K.; Tully, J. C.; Helfand, E. *J. Chem. Phys.* **1981**, *74*, 5300.
(32) Jansen, A. P. J. *J. Chem. Phys.* **1991**, *94*, 8444.
(33) Anderson, J. B. *J. Chem. Phys.* **1973**, *58*, 4684.
(34) Bonnet, L.; Rayez, J. C. *Chem. Phys. Lett.* **1997**, *277*, 183.
(35) Bonnet, L.; Rayez, J. C. *Chem. Phys. Lett.* **2004**, *397*, 106.
(36) Banares, L.; Aoiz, F. J.; Honvault, P.; Bussery-Honvault, B.; Launay, J. M. *J. Chem. Phys.* **2003**, *118*, 565.
(37) Banares, L.; Aoiz, F.; Vasquez, S. A.; Ho, T. S.; Rabitz, H. *Chem. Phys. Lett.* **2003**, *374*, 243.
(38) Pomerantz, A. E.; Ausfelder, F.; Zare, R. N.; Althorpe, S. C.; Aoiz, F. J.; Banares, L.; Castillo, J. F. *J. Chem. Phys.* **2004**, *120*, 3244.
(39) Banares, L.; Aoiz, F. J.; Honvault, P.; Launay, J. M. *J. Phys. Chem. A* **2004**, *108*, 1616.
(40) Balucani, N.; Capozza, G.; Cartechini, L.; Bergeat, A.; Bobbenkamp, R.; Casavecchia, P.; Aoiz, F. J.; Banares, L.; Honvault, P.; Bussery-Honvault, B.; Launay, J. M. *Phys. Chem. Chem. Phys.* **2004**, *6*, 4957.
(41) Xie, T.; Bowman, J.; Duff, J. W.; Braunstein, M.; Ramachandran, B. *J. Chem. Phys.* **2005**, *122*, 14301.
(42) Polanyi, J. C.; Wong, W. H. *J. Chem. Phys.* **1969**, *51*, 1439.
(43) Darling, G. R.; Holloway, S. *Surf. Sci. Lett.* **1992**, *268*, 305.
(44) Darling, G. R.; Holloway, S. *J. Electron Spectrosc. Relat. Phenom.* **1993**, *64*, 571.
(45) Perrier, A.; Bonnet, L.; Rayez, J. C. Manuscript in preparation, 2005.
(46) Bonnet, L.; Rayez, J. C. *Eur. Phys. J. D* **1998**, *4*, 169.
(47) Larregaray, P.; Bonnet, L.; Rayez, J. C. *J. Chem. Phys.* **2001**, *114*, 3349.
(48) Bonnet, L.; Larregaray, P.; Rayez, J. C. *J. Chem. Phys.* **2004**, *120*, 3665.
(49) Bonnet, L.; Larregaray, P.; Rayez, J. C. *J. Chem. Phys.* **2004**, *120*, 3679.
(50) Zare, R. N. *Angular Momentum: Understanding spatial aspects in chemistry and physics*; Wiley-Interscience: New York, 1988.